Proceedings of the IEEE International Conference on Image Processing, 16-19 September 1996, Lausanne Switzerland, pp. 637-640

DETERMINING LARGE SCALE SANDBAR BEHAVIOUR

Donald G. Bailey and Roger D. Shand

Image Analysis Unit and Geography Department
Massey University, Palmerston North, New Zealand
E-mail: D.G.Bailey@massey.ac.nz

ABSTRACT

To study the morphology of coastal sandbars and their change with time, it is necessary to obtain a sequence of maps over the period of interest. Traditional techniques such as vertical aerial photography or echo-sounding over a grid are expensive and subject to environmental constraints, especially in higher energy situations.

Image processing is used to rectify elevated terrestrial images where morphological features are inferred from breaking wave patterns. As the coordinates of interest are longshore and offshore distances, the image is then warped to make the coastline straight. The sandbar crest positions within this image are detected. An error analysis shows that useful quantitative data may be obtained. The temporal evolution of the bars can be identified from time stack images.

1. INTRODUCTION

A significant and increasing proportion of the worlds population and wealth is concentrated in the sand-dominated coastal zone [1]. This region, however, is highly variable and unstable with erosion exceeding deposition globally [2,3]. The predicted greenhouse associated sea-level rise is likely to exacerbate this situation [4,5]. There is clearly a practical need to maximise our understanding coastal systems.

Contemporary geomorphological field studies have tended to concentrate on the inner nearshore and backshore zones of low to moderate energy coasts [6], because of their relative ease of access.

To facilitate comprehensive nearshore investigations, in particular those on moderate to high energy coasts, methods of acquiring morphological data at a variety of scales, both spatial (10^1 to 10^{3+} metres longshore) and temporal (10^0 to 10^{3+} days), are required.

A variety of techniques have been used in the past for bathymetric sampling. Cost, longshore coverage limitations, and logistical problems prohibit the widespread use of bottom or surface moving instruments, especially in higher energy environments. Aerial imaging techniques increase longshore coverage but atmospheric restrictions (cloudless conditions) and high costs restrict the aerial (including satellite) option.

With the increasing power of personal computers, the use of image processing techniques now enables inexpensive morphological data to be obtained from elevated terrestrial surfzone images [7,8].

It is necessary to explore the limits and possibilities of the method with respect to the morphological scale objectives described above. This paper covers our image processing work and presents some of our preliminary results based on field data from Wanganui, New Zealand.

2. PREPROCESSING

A panorama of eight photographs was taken from a single site 150 m behind and 43 m above mean sea-level. The four central shots were taken using a 55 mm focal length lens to give good coverage of the area without sacrificing detail. To obtain satisfactory resolution for the four end shots, a 135 mm focal length lens was used. Each photograph was taken using a three minute time exposure to average the effects of individual waves.

A 512 x 512 image is captured of each photograph, with a 2:3 aspect ratio. While capturing the photographs, it is ensured that the top and bottom edges of the photographs are visible in the image since these are required for determining the camera tilt. It is also ensured that the left and right edges of the photographs are out of the field of view, otherwise artefacts may be introduced when mosaicing the photographs.

Since the panorama spans about 160° there is a considerable variation in lighting from one photograph to another because of differing sun angles. In addition to this, there may be sun glare from the sea or clouds and vignetting caused by the lens and neutral density filters. The first step is to normalise the contrast range of each image as much as possible.

1. The image is filtered by selecting the minimum pixel value within a 21 x 21 box. This effectively shrinks the lighter regions of the bars preventing them from being removed with the background.
2. This image is then filtered using the average within a 55 x 55 box to obtain an estimate of the local density. Variations in this image correspond to density variations in the original image.
3. The average is subtracted from the original image to remove the density variations. Differences in the range -12 to 80 are mapped to fill the available range (0 to 255) to enhance the contrast.

Figure 1 shows a typical contrast normalised image.

3. RECTIFICATION

Each photograph has perspective distortion resulting from the viewing geometry. This distortion must be removed before the individual photographs can be mosaiced to give the full panorama.

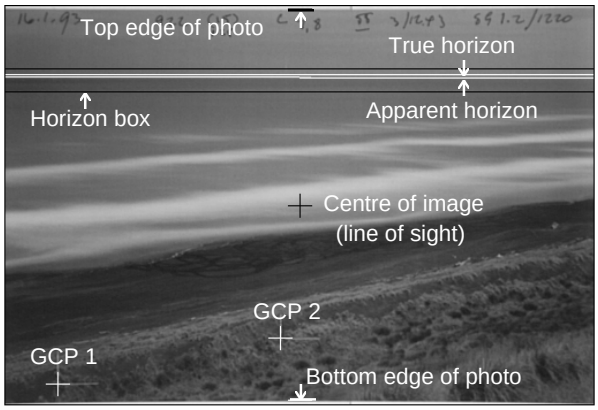

Figure 1: A typical contrast enhanced input image with key features labelled.

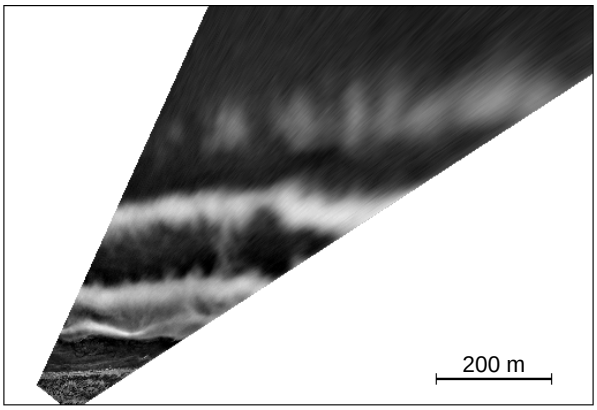

Figure 2: The perspective corrected image.

3.1 Correction of perspective distortion

At this stage, a convenient coordinate system is based on map coordinates. We have actually used rotated map coordinates since the stretch of coast under study runs SE to NW. If it is assumed that the earth is flat (a reasonable assumption since the ranges of interest are within 3.5 km from the camera location) the perspective correction equation may be represented by

$$X = \frac{a_0 x + a_1 y + a_2}{a_6 x + a_7 y + a_8}, \quad Y = \frac{a_3 x + a_4 y + a_5}{a_6 x + a_7 y + a_8} \qquad (1)$$

where (x,y) are the pixel coordinates in the image before rectification, and (X,Y) are the corresponding rectified coordinates. The 9 unknowns in equation (1) are solved from the camera position, the positions of two surveyed ground control points (GCPs) within each image, the sea level, and the horizon.

The common denominator of the perspective transformation represents the perspective vanishing line in the photographs:

$$a_6 x + a_7 y + a_8 = 0 \qquad (2)$$

If the earth was truly flat, this line would correspond to the horizon. However, because of the curvature of the earth, the visible horizon will be below the true "flat earth" horizon. Although the angle between them is small ($\theta = 0.21°$ for camera height of 43 m), this error is significant, giving a 4 pixel shift in the horizon for photographs taken using a 55 mm lens and a 9.5 pixel shift with a 135 mm lens.

From the positions of the ground control points in the image, the position of the apparent horizon is estimated. A linear edge detection operation is to detect the maximum intensity gradient within that region. A least squares fit is applied to the detected points to give the horizon. The program draws the detected horizon on the input image and asks the user if it has been detected correctly. If not, the user defines the correct horizon by entering two points. This step is necessary because the position of the horizon may not be detected accurately if the weather is hazy or if the sea has rough and calm patches on it.

The horizon is then corrected for θ to give a_6, a_7 and a_8. Note that equation (2) is normalised so that

$$a_6^{\,2} + a_7^{\,2} = 1 \qquad (3)$$

The next step is to reference the camera and ground control points to sea level. The GCPs are projected to sea level to remove their height, giving coordinates (X_1',Y_1') and (X_2',Y_2').

Lines perpendicular to the horizon on the input image all fall on planes which pass through the camera. Therefore these lines all converge at the camera point in the rectified image. If the camera is tilted so that the line of sight is below the true horizon, the point of intersection of the horizon perpendiculars will move behind the camera. Determining the seal-level referenced camera position requires knowing the line of sight.

It is assumed that the pixel mid way between the top and bottom edge of the photograph is along the line of sight of the camera. The tilt, φ, is calculated from the focal length and position of the horizon in the image. The direction of the line of sight is calculated by solving equation (1) assuming no tilt (using actual camera coordinates (X_c,Y_c)). The centre pixel of the image is then transformed to give the direction of the line of sight, γ. This is used to correct the camera position for' tilt (equation 4) and equation (1) is solved again.

$$X_c^{'} = X_c - Z_c \tan\varphi \sin\gamma, \quad Y_c^{'} = Y_c - Z_c \tan\varphi \cos\gamma \qquad (4)$$

Lines perpendicular to the horizon intersect at the corrected camera position after transformation. These lines may be parameterised by

$$x = a_6 t + b_0, \quad y = a_7 t + b_1 \qquad (5)$$

where b_0 and b_1 are arbitrary constants. Substituting these into equation (1) gives

$$\begin{aligned} X_c^{'} &= \underset{t\to\infty}{Limit} \frac{a_0(a_6 t + b_0) + a_1(a_7 t + b_1) + a_2}{a_6(a_6 t + b_0) + a_7(a_7 t + b_1) + a_8} \\ &= \frac{a_0 a_6 + a_1 a_7}{a_6^{\,2} + a_7^{\,2}} = a_0 a_6 + a_1 a_7 \end{aligned} \qquad (6)$$

Each GCP gives a further independent equation in a_0, a_1 and a_2, as in equation (7)

$$X_1^{'} = \frac{a_0 x_1 + a_1 y_1 + a_2}{a_6 x_1 + a_7 y_1 + a_8} = \frac{a_0 x_1 + a_1 y_1 + a_2}{H_1} \qquad (7)$$

where H_1 is a constant (all its terms are known). Equation (6) and equation (7) for each GCP give three simultaneous equations that are solved to give

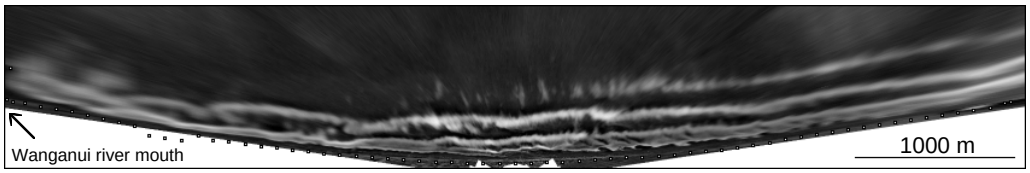

Figure 3: Mosaic of 8 perspective corrected images.

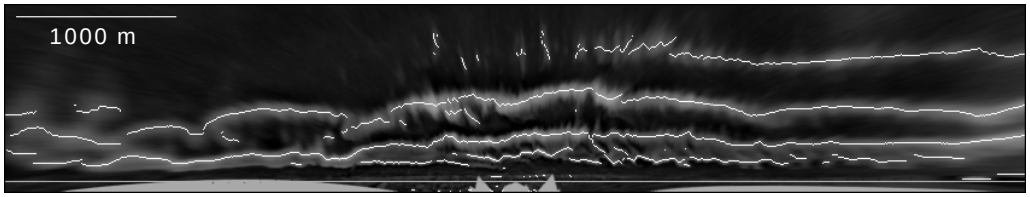

Figure 4: Detected sandbars and waterline (offshore distance scale x2)

$$a_0 = \frac{X_c'(y_1 - y_2) - a_7(H_1X_1' - H_2X_2')}{a_6(y_1 - y_2) - a_7(x_1 - x_2)}$$
$$a_1 = \frac{a_6(H_1X_1' - H_2X_2') - X_c'(x_1 - x_2)}{a_6(y_1 - y_2) - a_7(x_1 - x_2)} \quad (8)$$
$$a_2 = X_1'H_1 - a_0x_1 - a_1y_1$$

Similar equations may be obtained for a_3, a_4 and a_5. Equation (1) is then used to transform each pixel in the input image, giving figure 2. The transformed image is sampled with 2 metre resolution.

3.2 Mosaicing

After correcting for perspective distortions in each of the eight input photographs, the images are combined into a single view of the coast. The views provided by the individual photographs overlap slightly. To reduce the possibility of artefacts from the joins, the images are merged using a linear transition in the region of overlap between adjacent views. The resulting mosaic is shown in figure 3.

3.3 Straightening of coastline

In determining the positions of the bars, a more useful coordinate system is longshore and offshore coordinates. To facilitate conversion to these coordinates, a separate series of ground control points was surveyed along the toe of the foredune at 100m intervals. These points define the baseline for offshore distance measurements. A least squares parabolic fit is made over 1000 m sections, with 500 m overlap between the sections. The overlapping regions are combined using a linear spline giving a smooth piecewise cubic fit.

The image is then incrementally rotated (or unrolled) to make the baseline straight. At each point along the baseline, the shore normal is calculated and the image resampled along the shore normal. Having the offshore and longshore variations separated enables the offshore scale to be amplified to highlight the sandbar morphology.

4. DETECTION OF SANDBARS

The positions of the bar crests can be inferred from the position of maximum intensity along the bar. Although not completely accurate (since the position of maximum intensity depends on environmental factors such as tide, wind and wave height) this measure provides the best estimate from the information available. The following steps are used to detect the bar crests:

1. The image is filtered to detect the local maximum pixels using a 1 x 21 pixel box. The maxima are coded with their pixel values.
2. Many of the local maxima detected correspond to noise, so the image is thresholded at a pixel value of 80 to select only the significant maxima, corresponding to the bar crests.
3. Finally the detected crests are thinned to a single pixel thickness. The resulting image is shown in figure 4 overlaid on the original.

Quantitative measurements may be made of the bar positions by measuring the offshore distances of the intensity maxima from the baseline.

5. RESULTS

The elevated terrestrial imaging approach described here provides good accuracy (±10m) in the offshore direction, but deteriorates rapidly in the longshore direction with distance from the camera. There are three main sources of longshore error which all vary approximately linearly with distance: resolution of captured images (±40m at 3km); photogrammetric errors (±60m at 3km) and blur caused by the height of the waves (±75m at 3km). As these sources are independent, the corresponding variances have been added to give a longshore error of ±2m directly out from the camera up to ±100m at a distance of 3km. The effect of deteriorating resolution with range can be seen in figures 3 and 4.

In addition to these, the intensity maxima shift as a function of environmental variables (tide, wind and wave height). This shift can be reduced by longshore averaging during image processing. The shift in maxima ranged from ±15m when averaging over 200 m up to ±35m for narrow offshore transits. The averaging process effectively trades longshore morphological detail for offshore accuracy. Field work by Lippmann and Holman at Duck indicates that the actual bar crest is likely to be in this range [7].

An ongoing data gathering program has been established consisting of four years of nearshore activity captured at monthly intervals. The temporal resolution of this data allows seasonal variations to be determined. In addition, a weekly data set over a two year period allows the effects of individual weather patterns to be determined.

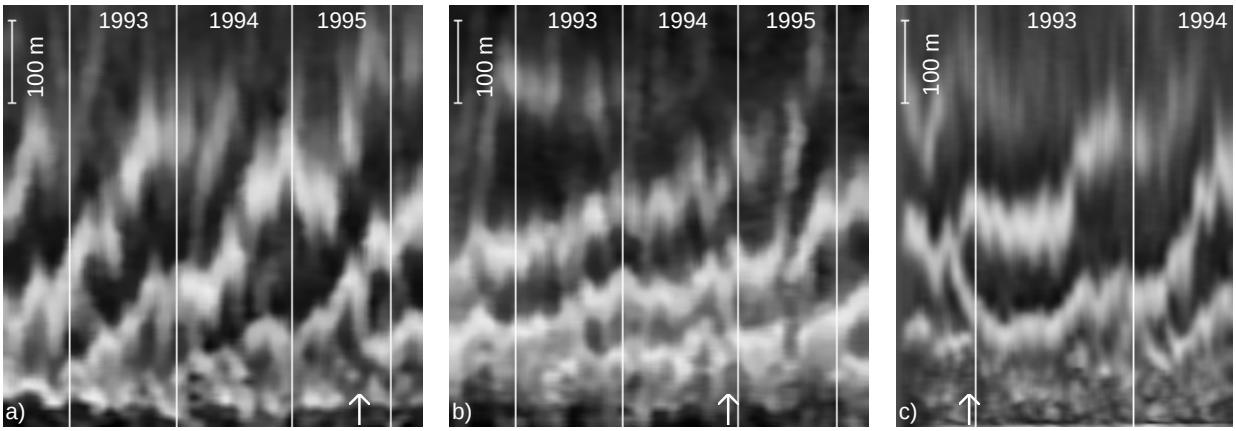

Figure 5: Time-stacks showing bar movements and bifurcation. a) Four year monthly series at 1500 m from river mouth b) Four year monthly series at 6000 m from river mouth; c) Two year weekly series at 3500 m from river mouth.

The morphodynamic evolution of the sandbars is investigated by examining the positions of the bars detected in a series of images taken at regular intervals. This three dimensional data set (offshore, longshore, and time coordinates) may be viewed as a series of time-stack images with offshore and time axes. Each time-stack shows bar behaviour at a particular longshore location as a function of time. Figure 5 shows three time-stacks at different locations and temporal sampling resolution.

A number of new morphological phenomena have been identified. The bars can be observed to have an underlying offshore migration trend with weak seasonal cycles superimposed on this. Such behaviour is easily recognised on the time-stack images in figure 5. It can be clearly seen that the bars closer to the river mouth (for example figure 5a) have a stronger seasonal cycle, with offshore movement occurring predominantly in the winter months when the energy within the system is higher. Comparing time-stacks for different longshore locations (figures 5a and 5b) also shows that the average offshore migration rates are faster nearer the river mouth.

A second characteristic involves bars splitting or bifurcating longshore. Examples appear in each time-stack in figure 5 as marked by the arrows. In each case, the inner portion moved landward to merge with the beach or adjacent bar. This could be an important sediment return mechanism. Similar bifurcations can be seen in figure 4 where they occur at approximately 1000 m intervals.

6. SUMMARY

An inexpensive method of obtaining data for studying the time evolution of sandbars on moderate to high energy coasts is to use elevated terrestrial imaging. A panoramic series of eight oblique photographs are normalised with respect to lighting variations and rectified to longshore and offshore coordinates. The positions of the bar crests are detected by the locating intensity maxima. An error analysis for this study site shows that quantitatively useful data may be obtained. Time-stack images may be used to show how the bars evolve over several seasons.

7. ACKNOWLEDGMENTS

We acknowledge financial support for the project from the Massey University Graduate Research Fund, the Massey University Research Fund, and the Geography Department. We also acknowledge field assistance in surveying the ground control points from the Wanganui District Council.

REFERENCES

[1] **R.W.G. Carter.** Man's Response to Sea-Level Change. In R.J.N. Devoy, editor, *Sea Surface Studies: A Global View*, 464-497, Croom Helm, London, 1987.

[2] **R.W.G. Carter.** *Coastal Environments.* Academic Press, London, 1988.

[3] **E.C.F. Bird.** *Coastline Changes: A Global View*. John Wiley & Sons, London, 1985.

[4] **J. Orford.** Coastal Processes: The Coastal Response to Sea-Level Variation. In R.J.N. Devoy, editor, *Sea Surface Studies: A Global View*, 415-451. Croom Helm, London, 1987.

[5] **H.A. Viles.** The Greenhouse Effect, Sea-Level Rise and Coastal Geomorphology. *Progress in Physical Geography*, 13:452-461, 1989.

[6] **G. Masselink and A.D. Short.** The Effect of Tide Range on Beach Morphodynamics and Morphology: A Conceptual Beach Model. *Journal of Coastal Research*, 9:785-800, 1993.

[7] **T.C. Lippmann and R.A. Holman.** Quantification of Sand Bar Morphology: A Video Technique Based on Wave Dissipation. *Journal of Geophysical Research*, 94(C1): 995-1011, 1989.

[8] **D.G. Bailey and R.D. Shand.** Determining Large Scale Sandbar Evolution, *Proceedings of the First New Zealand Conference on Image and Vision Computing*, 109-116, 1993.